THE ASTROPHYSICAL JOURNAL, 436:654–668, 1994 December 1


# VLA OBSERVATIONS OF THE RICH X-RAY CLUSTER ABELL 2256

H. RÖTTGERING,[1,2,3] I. SNELLEN,[1] G. MILEY,[1] J. P. DE JONG,[1] R. J. HANISCH,[4] AND R. PERLEY[5]
*Received 1994 February 18; accepted 1994 May 24*

## ABSTRACT

The complex radio emission from the rich X-ray cluster of galaxies Abell 2256 has been mapped at 20 cm using the VLA in A, B, C, and D configurations and at 90 cm using the VLA in B configuration. The observations give detailed information about radio structures on scales up to 10 arcminutes with an angular resolution of 1".5 and with an unprecedented signal-to-noise ratio. The properties of the northern radio halo, the numerous head-tail sources and a unique ultra-steep spectrum source are discussed, taking into account the recent results of the *ROSAT* X-ray satellite.

The northern halo of Abell 2256 has a remarkable morphology. It has sharp edges and possible filamentary structure. The origin of this halo is discussed. We suggest that the region contains two or three head-tail galaxies that are heavily distorted due to the infalling subcluster that has been inferred from the *ROSAT* data. We find that one radio tail extends to at least about 700 kpc from its parent galaxy and seems morphologically disconnected from the cluster halo. From the small deviations from the remarkable straightness of this source, we estimate the turbulence in the confining X-ray gas around this source to be $\sim 200$ km s$^{-1}$ on scales of about 20 kpc.

The nature of the ultrasteep spectrum source is unclear. The source, with a spectral index of $-1.6$, has a Z-shaped morphology and is extended by $\sim 4'$. We tentatively identify it with a cluster galaxy coincident with the eastern "flatter" region. The ultrasteep spectrum source may be a head-tail radio galaxy with peculiar morphology.

The overall conclusion from the radio data is that the remarkable radio properties of Abell 2256 can be explained within the merging subcluster model as due to both the high velocity dispersion of the cluster galaxies and the high gas density of the intercluster medium which both contribute to shaping the radio morphologies.

*Subject headings:* galaxies: clusters — radio continuum: galaxies — X-rays: galaxies

## 1. INTRODUCTION

Abell 2256 is an exceptional cluster of galaxies at a redshift of 0.06. There are several optical properties which distinguish it from the majority of clusters in the Abell catalog. First, its radial velocity dispersion is 1300 km s$^{-1}$, ranking it among the largest observed for any cluster (Faber & Dressler 1977; Fabricant, Kent, & Kurtz 1989; Bothun & Schombert 1990). Second, it is among the richest 5% of clusters in the Abell Catalogue and has an extremely low fraction of spiral galaxies (9% $\pm$ 6%, Butcher & Oemler 1978).

Abell 2256 is also notable for its extreme X-ray properties. The X-ray emission is among the most powerful ($\sim 10^{45}$ ergs s$^{-1}$), and hottest (7 keV) of all known clusters (Mushotzky et al. 1978; Forman & Jones 1982; David et al. 1993). The *ROSAT* X-ray images show two separate peaks of emission that have different temperatures indicating that in Abell 2256 a subcluster may be merging with a larger cluster (Briel et al. 1991).

At radio wavelengths Abell 2256 is truly remarkable. The Westerbork radio maps at 20 and 50 cm wavelength show a wide variety of radio structures (Bridle & Fomalont 1976; Bridle et al. 1979; Jägers 1986). The cluster contains at least four galaxies having head-tail morphologies, more than any other known cluster, a 4′ optically unidentified radio source with an ultrasteep spectrum ($\alpha \sim -1.6$), and two regions of extended "halo" emission. Abell 2256 can therefore be considered as an important object for studying the origin of several fundamental astrophysical phenomenon.

Here we report on radio maps of Abell 2256 made at 20 cm using the VLA in A, B, C, and D configurations and at 90 cm using the VLA in B configuration. Our purpose in carrying out these observations was to study the exceptional radio emission in more detail than had been done previously and to compare the radio properties with the anomalous characteristics of Abell 2256 at other wavelength regions. In particular, we hoped (1) to determine the nature of the 4′ ultrasteep spectrum source, (2) to find some clues about the origin of the radio halo, and (3) to find additional distinct properties of the cluster that would explain why the cluster is such a good spawning ground for head-tail radio sources.

The data presented here are particularly relevant for comparison with the recently published *ROSAT* observations of Abell 2256. We shall show that there is morphological evidence for a connection between the radio and X-ray emission.

The structure of this paper is as follows. We shall first present the observations and the radio maps that we have obtained. In the discussion thereafter we shall focus on three issues: (1) the connection between the radio and the X-ray emission, (2) the origin of the northern radio halo, and (3) the nature of the most extreme head-tail source.

[1] Leiden Observatory, P.O. Box 9513, 2300 RA, Leiden, Netherlands.
[2] Mullard Radio Astronomy Observatory, Cavendish Laboratory, Madingley Road, Cambridge, CB3 0HE, England.
[3] Institute of Astronomy, Madingley Road, Cambridge, CB3 0HA, England.
[4] Space Telescope Science Institute, 3700 San Martin Dr., Baltimore, MD 21218.
[5] National Radio Astronomy Observatory, P.O. Box O, Socorro, NM 87801.

TABLE 1

RELEVANT PARAMETERS OF THE VLA OBSERVATIONS

| Date | Configuration | Frequency (GHz) | Bandwidth (MHz) | Visibility Averaging Time (s) | Spatial Scales | Total Integration Time |
|---|---|---|---|---|---|---|
| 1990 Mar 27 ..... | A | 1.44615 | 15 × 2 × 1.5625 | 5 | 1″.4–30″ | $7^h55^m$ |
| 1987 Dec 26 ..... | B | 1.44615 | 2 × 12.5 | 10 | 4″–1′.3 | 8 20 |
| 1988 Mar 15 ..... | C | 1.44615 | 2 × 12.5 | 20 | 13″–4′.5 | 8 10 |
| 1988 Sep 2 ..... | D | 1.44615 | 2 × 12.5 | 30 | 44″–15′ | 7 55 |
| 1990 Aug 6 ..... | B | 0.32750 | 2 × 12.5 | 10 | 21″–7′ | 8 28 |

Throughout this paper we shall assume a Hubble constant of 50 km $s^{-1}$ $Mpc^{-1}$, placing Abell 2256 at a distance of 340 Mpc. The corresponding linear/angular scale conversion at Abell 2256 is then 1.65 kpc $arcsec^{-1}$.

## 2. OBSERVATIONS AND REDUCTION

Abell 2256 was observed at 20 cm using the VLA in A, B, C, and D configurations, and at 90 cm using the VLA in B configuration. Relevant parameters of the observations are listed in Table 1. For the 20 cm observations the sources 3C 286 and 2007+776 were used as primary amplitude calibrators and for the 90 cm observations the sources 3C 286 and 3C 48. The 20 cm A-configuration observations were taken in spectral line mode to eliminate the effects of bandwidth smearing.

Except for the special software that we used in the reduction of the 90 cm data, all the reduction was performed using the AIPS image processing system developed by the National Radio Astronomy Observatory.

The maps for the 20 cm B-, C-, and D-configuration data were produced and cleaned using the ungridded subtraction method (Schwab 1984) as implemented in the AIPS task MX. Self-calibration (Cornwell & Wilkinson 1981) was applied with two iterations on the phases alone and one on both phases and amplitude. A map was made from the self-calibrated data from the C and D configurations by reducing the combined C + D *uv* data in the same way as for the visibilities from individual configurations.

Because of the large number of independent *uv* data points the analysis of the 20 cm A-array data is demanding. Therefore the reduction was carried out as follows. Initial maps were made from the *uv* data from each of the individual frequency channels and were cleaned in a standard way. To minimize demands on the available computer resources, self-calibration was applied only once on the phases, using as a model the average of the 15 initial maps. The final map (map 20A) was obtained by averaging the individual channel maps that were made from the self-calibrated data.

The 90 cm data were only recently reduced. Although careful spectral comparison will only be possible after 90 cm data at different VLA configurations have been obtained, we regard these first results to be worthy of mentioning at this stage. For the 90 cm data, we used special software (the polyhedron method) to correct the maps for aberrations caused by the "depth" (three-dimensional effect) of the array (Cornwell & Perley 1992).

The characteristics of the resulting maps are given in Table 2.

## 3. RADIO MAPS

To show optimally the huge diversity of radio structures in Abell 2256, several sections of the maps (e.g., Table 2) are presented in what follows.

### 3.1. *Overview and Source Description*

An overall impression of the cluster as a whole is given in Figure 1. This 20 cm map that shows structures with spatial scales ranging from 13″–15′ (map 20CD) is a combination of the C + D data.

In Figure 2 we show the central part of the 90B map. The sources with a steep spectral index are clearly more prominent in this map than in the 20 cm map.

Sources with a peak brightness larger than 1 mJy $beam^{-1}$ on map 20CD within a distance of 22′.5 from the pointing center of the observations ($17^h06^m$, 78°45′, B1950) are listed in Table 3. This combination of peak brightness limit and radius has been chosen so that a slightly resolved source at the edge of the field (where the noise corresponds to ~0.1 mJy $beam^{-1}$ due to the decreased sensitivity of the primary beam) with a peak brightness of 1 mJy $beam^{-1}$ in the 20CD map will have a peak brightness in the 20B map of $\gtrsim 1\ \sigma$ above the local background rms. The sources are labeled A–M according to the convention of Bridle et al. (1979). In addition we also list component F1, the only source in the list of Bridle et al. (1979) that did not satisfy our selection criteria. The remaining sources are listed in order of peak flux density (in the 20CD map) and are labeled N–AF.

The coordinates, peak brightness, angular sizes, and position angles have been found by fitting an elliptical Gaussian func-

TABLE 2

PARAMETERS OF THE VLA MAPS

| Map Name | VLA Configuration | Frequency (GHz) | Clean Beam | Map Size | RMS Noise in Center (μJy/beam) |
|---|---|---|---|---|---|
| 20A ..... | A | 1.44615 | 1″.4 × 1″.2 | 14′ × 14′ | 50 |
| 20B ..... | B | 1.44615 | 4.5 × 3.9 | 51 × 51 | 40 |
| 20CD ..... | CD | 1.44615 | 17.3 × 13.7 | 85 × 85 | 40 |
| 90B ..... | B | 0.32750 | 21.8 × 20.1 | 315 × 315 | 390 |

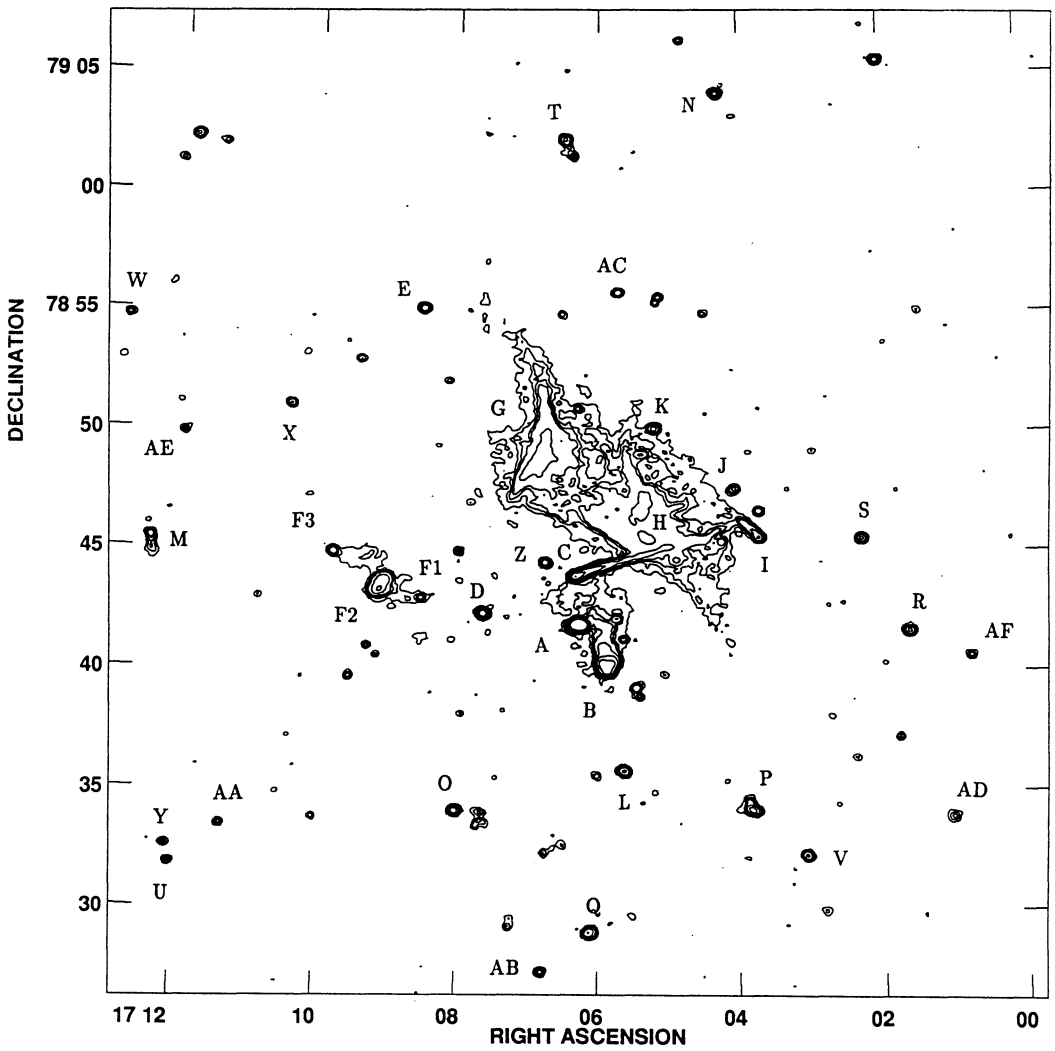


FIG. 1.—Abell 2256 at 1.4 GHz (central region of map 20CD) showing emission on scales from 13″ to 15′. The contours are at 50 × (−3, 3, 6, 9, 12, 24, 48, 96, 192) $\mu$Jy beam$^{-1}$.

tion to the brightness maxima of the sources on the 20B map. For the well-resolved sources (>20″), the angular sizes and the position angles were measured from the location of the source extremities. The total flux densities at 20 and 90 cm have been obtained by integrating the flux densities on the 20CD and 90B maps within boxes around the sources. The errors of the integrated flux densities have been determined assuming Poissonian noise with these boxes. The resulting two-point spectral index is also listed. Since the 20CD data are deeper and more sensitive to extended structure than the 90B data (see Tables 1 and 2), some of the spectral indices of the larger sources might not be correct. To estimate the amount of flux that might have been missed in the 90B data, we calculate an upper limit to the 90 cm flux taking into account the noise on the 90B map within the aperture that we used for the 20 cm flux measurements. The combination of this upper limit plus the limits from the errors for the integrated fluxes give the acceptable range for the spectral indices. Since sources J, AC, AE, and AF are not detected at 90 cm, we only list upper limits of the spectral index.

Sources with an optical identification are indicated by the flag " + " in Table 3 and sources that have a tentative identification are indicated by the flag " ?." The optical identifications for the sources A–M were taken from Bridle et al. (1979). Note that Bridle et al. did not find an optical counterpart to the sources F1 and F2 down to the limits of the Palomar Sky Atlas. For the sources L and M, the difference between our VLA radio positions and the optical positions as given by Bridle et al. (1979) are, respectively, 15″ and 20″, and we therefore regard the identifications of Bridle et al. (1979) as tentative. In the spectroscopic survey of cluster members of Fabricant et al. (1989) which is complete to $r$ magnitudes of 16.8, we searched for identifications of the sources N–AF. Sources AC, AD, and AE were identified with cluster galaxies. The position difference between source AA and galaxy number 135 from the list of Fabricant et al. (1989) was 21″, and therefore we considered this identification as unreliable.

### 3.2. *The Head-Tail Sources*

The four radio sources that have their radio emission preferentially on one side of the optical identification were classified as head-tail galaxies. This is indicated by the flag " h " in Table 3. We confirm the conclusion of Bridle et al. (1979), that the

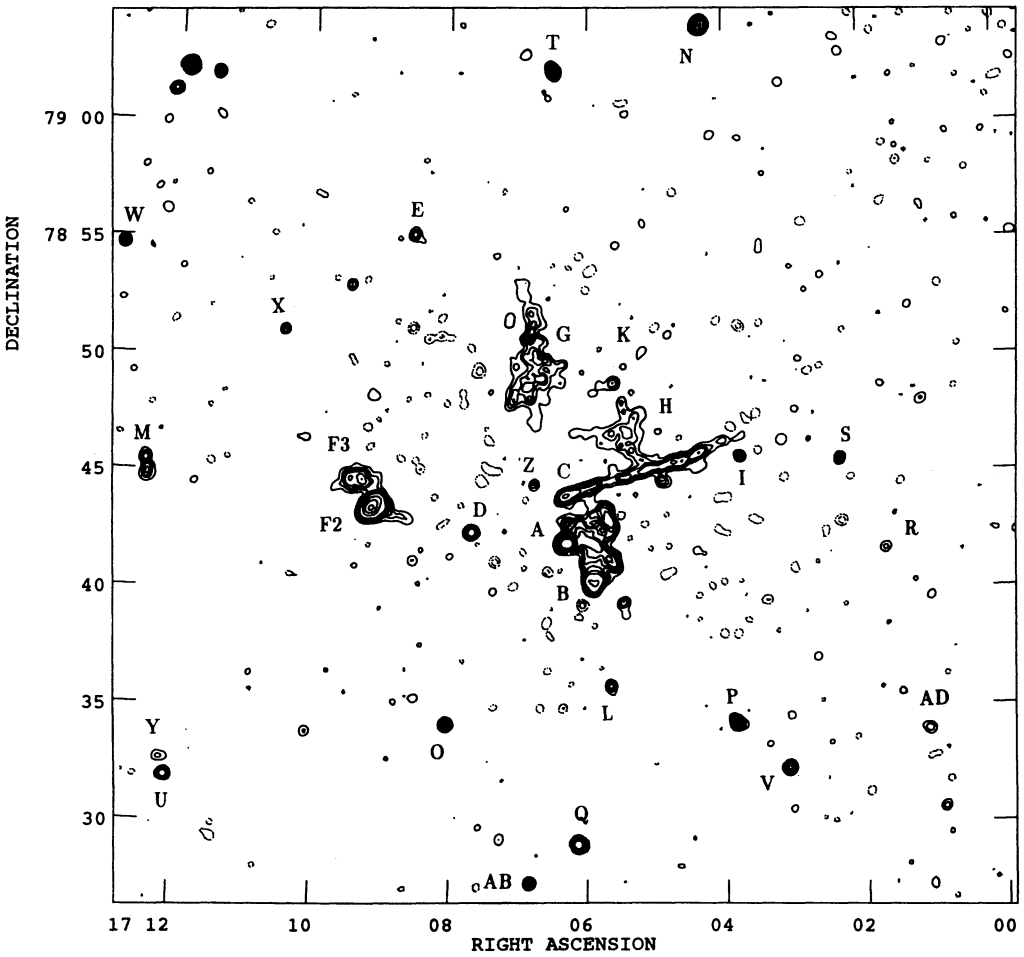


FIG. 2.—Abell 2256 at 0.3 GHz (B configuration). The contours are at 500 × (−6, −3, 3, 6, 9, 12, 18, 24, 48, 72, 96) μJy beam$^{-1}$. The gray-scale ranges in brightness from 0 to 20 μJy beam$^{-1}$.

radio sources A, B, C, and I are definite head-tail galaxies. In Figures 3, 4, 5, and 6 radio maps for the head-tailed sources A, B, C, and I are presented.

Source B is a prime example of a head-tail galaxy. It resembles NGC 1265, the well-studied head-tail galaxy in the Perseus cluster (e.g., Miley, Wellington, & van der Laan 1975; O'Dea & Owen 1986). Source C has a remarkably straight, narrow, and long appearance. Its length of 425″ as measured from the 20CD map corresponds to 700 kpc at the distance of the cluster. Note, however, that the observed tail length is a function of observing frequency, *uv* coverage, resolution, and sensitivity. If this object is indeed a head-tail, its length classifies it among the longest head-tail sources known. In the list of 51 head-tails of O'Dea & Owen (1985b) only two head-tails are longer. One of these is 1709+397 (~750 kpc, Miley & Harris 1977), but is not so straight and well confined. The other is 1132+492 (Valentijn 1979; O'Dea & Owen 1985a), which is considerably wider (20 kpc) than source C. The peak of the emission of source C coincides with a magnitude 15.3 optical galaxy (Bridle et al. 1979). Both the 20 and 90 cm brightness decrease rapidly with distance from the optical galaxy (Fig. 7) and we observe clear spectral steepening, with the spectral

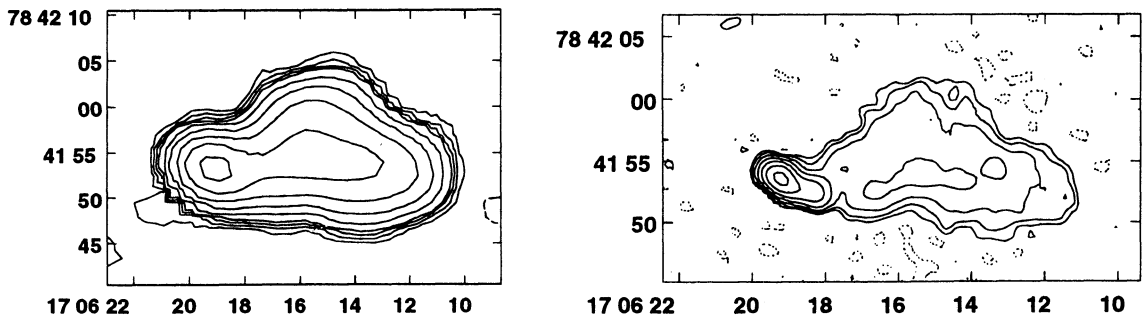


FIG. 3.—*Left*: Source A on map 20B. The contours are at 50 × (−3, 3, 6, 9, 12, 24, 48, 96, 192, 384) μJy beam$^{-1}$. *Right*: Source A on map 20A. The contours are at 50 × (−3, 3, 6, 9, 12, 24, 48, 96, 192, 384) μJy beam$^{-1}$.

TABLE 3

OBSERVED PARAMETERS OF THE RADIO SOURCES

| Component | R.A. (1950) | Decl. (1950) | 20 cm Peak Brightness (mJy/beam) | 20 cm Integrated Flux Density (mJy) | 90 cm Peak Brightness (mJy/beam) | 90 cm Intrgrated Flux Density (mJy) | Spectral Index | Angular Size | P.A. | ID | Morphology |
|---|---|---|---|---|---|---|---|---|---|---|---|
| A ..... | 17h 6m19s.2 | 78°41'52".4 | 14.4 | 122.1 ± 3.6 | 220 | 402 ± 24 | $-0.79^{+0.05}_{-0.06}$ | 20" | −90° | + | h |
| B..... | 17 5 51.3 | 78 39 54.4 | 2.1 | 60.5 ± 7.1 | 26 | 273 ± 28 | $-1.00^{+0.15}_{-0.15}$ | 130 | 0 | + | h |
| C ..... | 17 6 20.6 | 78 43 51.6 | 3.6 | 46.0 ± 5.6 | 28 | 246 ± 20 | $-1.11^{+0.14}_{-0.15}$ | 425 | −72 | + | h |
| D ..... | 17 7 38.6 | 78 42 22.6 | 4.7 | 11.8 ± 0.6 | 19 | 22 ± 2 | $-0.41^{+0.10}_{-0.10}$ | 9 | 22 | + | ... |
| E..... | 17 8 30.6 | 78 55 5.9 | 2.1 | 4.5 ± 0.7 | 7 | 13 ± 1 | $-0.71^{+0.15}_{-0.15}$ | 6 | 42 | + | ... |
| F1 ..... | 17 5 9.3 | 78 45 32.0 | 03 | 3.6 ± 1.2 | 9 | 25 ± 6 | $-1.29^{+0.36}_{-0.46}$ | 20 | 82 | ... | ... |
| F2 ..... | 17 9 6.3 | 78 43 27.9 | 0.5 | 23.6 ± 1.5 | 51 | 250 ± 18 | $-1.57^{+0.12}_{-0.12}$ | 36 | −41 | ... | ... |
| F3 ..... | 17 9 44.2 | 78 44 50.6 | 0.3 | 11.4 ± 3.2 | 11 | 78 ± 10 | $-1.28^{+0.21}_{-0.30}$ | 17 | −65 | + | ... |
| G ..... | 17 6 39.2 | 78 54 0.8 | 0.2 | 153 ± 40 | 7 | 265 ± 57 | $-0.37^{+0.32}_{-0.57}$ | 375 | ... | + | ... |
| H ..... | 17 5 23.4 | 78 46 40.5 | 0.1 | 102 ± 45 | 6 | 159 ± 35 | $-0.30^{+0.35}_{-0.65}$ | 210 | ... | ... | ... |
| I ..... | 17 3 42.7 | 78 45 29.6 | 1.7 | 8.2 ± 1.8 | 6 | 8 ± 1 | $+0.02^{+0.25}_{-0.52}$ | 75 | 45 | + | h |
| J ..... | 17 4 3.9 | 78 47 34.8 | 1.7 | 2.1 ± 0.3 | ... | <1 | >0.4 | 5 | −82 | + | ... |
| K ..... | 17 5 12.0 | 78 50 5.8 | 0.6 | 3.4 ± 0.3 | 3 | 7 ± 1 | $-0.48^{+0.18}_{-0.17}$ | 8 | 7 | + | ... |
| L..... | 17 5 37.2 | 78 35 50.0 | 1.0 | 5.3 ± 0.3 | 7 | 7 ± 1 | $-0.18^{+0.16}_{-0.16}$ | 20 | 62 | ? | ... |
| M..... | 17 12 23.1 | 78 45 11.6 | 0.5 | 10.7 ± 2.7 | 8 | 36 ± 6 | $-0.81^{+0.27}_{-0.25}$ | 60 | −63 | ? | ... |
| N ..... | 17 4 18.3 | 79 4 6.7 | 6.0 | 12.4 ± 0.8 | 39 | 66 ± 4 | $-1.11^{+0.08}_{-0.07}$ | 9 | −29 | ... | ... |
| O ..... | 17 8 1.3 | 78 34 9.17 | 4.3 | 7.4 ± 0.3 | 15 | 16 ± 1 | $-0.51^{+0.05}_{-0.06}$ | 6 | −33 | ... | ... |
| P..... | 17 3 49.3 | 78 34 13.8 | 2.2 | 11.0 ± 2.1 | 15 | 22 ± 4 | $-0.46^{+0.22}_{-0.25}$ | 30 | 56 | ... | ... |
| Q ..... | 17 6 6.1 | 78 29 4.9 | 1.5 | 9.8 ± 0.3 | 20 | 39 ± 3 | $-0.92^{+0.09}_{-0.08}$ | 14 | −19 | ... | ... |
| R ..... | 17 1 37.2 | 78 41 39.5 | 3.4 | 6.5 ± 0.3 | 4 | 6 ± 1 | $+0.05^{+0.17}_{-0.15}$ | 7 | 84 | ... | ... |
| S ..... | 17 2 16.7 | 78 45 30.7 | 3.5 | 4.5 ± 0.3 | 7 | 7 ± 1 | $-0.29^{+0.15}_{-0.15}$ | 6 | −90 | ... | ... |
| T..... | 17 6 28.4 | 79 2 9.9 | 1.0 | 6.8 ± 2.2 | 13 | 21 ± 4 | $-0.75^{0.21}_{-0.24}$ | 65 | 27 | ... | ... |
| U ..... | 17 12 2.4 | 78 31 51.4 | 1.3 | 4.9 ± 0.3 | 9 | 14 ± 1 | $-0.70^{+0.14}_{-0.15}$ | 13 | −48 | ... | ... |
| V ..... | 17 3 4.2 | 78 32 18.1 | 0.8 | 4.7 ± 0.3 | 12 | 17 ± 2 | $-0.85^{+0.14}_{-0.16}$ | 13 | 30 | ... | ... |
| W..... | 17 12 45.8 | 78 54 42.1 | 0.9 | 4.0 ± 0.3 | 8 | 12 ± 1 | $-0.73^{+0.17}_{-0.18}$ | 13 | 50 | ... | ... |
| X ..... | 17 10 24.3 | 78 51 3.7 | 1.4 | 2.6 ± 0.3 | 5 | 5 ± 1 | $-0.43^{+0.24}_{-0.24}$ | 7 | 73 | ... | ... |
| Y ..... | 17 12 6.1 | 78 32 36.6 | 1.0 | 4.4 ± 0.3 | 4 | 9 ± 1 | $-0.48^{+0.16}_{-0.16}$ | 11 | −57 | ... | ... |
| Z..... | 17 6 44.8 | 78 44 28.2 | 2.1 | 2.8 ± 0.3 | 5 | 5 ± 1 | $-0.39^{+0.14}_{-0.14}$ | 5 | 68 | ... | ... |
| AA..... | 17 11 20.2 | 78 33 30.3 | 1.0 | 2.8 ± 0.3 | 3 | 8 ± 1 | $-0.70^{+0.11}_{-0.11}$ | 8 | −74 | ? | ... |
| AB..... | 17 6 47.5 | 78 27 26.5 | 0.6 | 3.3 ± 0.3 | 7 | 11 ± 1 | $-0.80^{+0.17}_{-0.17}$ | 10 | −55 | ... | ... |
| AC..... | 17 5 43.1 | 78 55 47.0 | 1.4 | 2.1 ± 0.3 | ... | <1 | >0.4 | 6 | −10 | + | ... |
| AD ..... | 17 1 2.4 | 78 33 54.7 | 0.4 | 4.2 ± 0.3 | 4 | 6 ± 1 | $-0.24^{+0.19}_{-0.18}$ | 18 | 46 | + | ... |
| AE..... | 17 11 56.3 | 78 49 51.8 | 0.6 | 2.2 ± 0.3 | ... | <1 | >0.4 | 8 | 84 | + | ... |
| AF..... | 17 0 45.4 | 78 40 37.4 | 0.6 | 2.1 ± 0.3 | ... | <1 | >0.4 | 8 | 76 | + | ... |

index varying from $\alpha = -0.6$ near the head to $\alpha \lesssim -1.3$ at the end of the tail. Similar spectral steepening has been observed in other head-tail sources such as 3C 129 (e.g., Jaffe & Perola 1973). In addition, the brightness at 90 cm appears to be modulated along the tail with a period of ~50". This modulation is also reflected in the spectral index distribution along the tail (e.g., Fig. 7). It is not clear, however, if our 90 cm B-configuration data have sufficient *uv* coverage to conclude that these "quasi-periodic" variations are real.

Source C is extremely straight: in map 20B the relative transverse position of the peak of the emission varies by only a few arcseconds over the first 250" (~10 kpc over ~410 kpc; e.g., Fig. 8). Just beyond a point ~350" from the head, the tail suddenly bends by ~10°–15° (e.g., Fig. 6). The width of source C is unresolved in the 20B map until a distance of 3' away from the galaxy. Thereafter there is some evidence that it slightly widens, although the signal to noise in this region is poor (e.g., Fig. 8). In the 20A map we only have enough signal-to-noise to determine the width of the tail up to distance of ~25" from the galaxy. The tail is unresolved over this distance in the 20A map, indicating that the transverse width is less than 1".5 (~2.5 kpc).

### 3.3. *Uptrasteep Spectrum Source "F"*

Although source F3 satisfies our definition of a head-tail, we hesitate to classify it as such. Source F3 is probably related to F1 and F2, making the whole source F is very unusual.

In Figure 9 we present maps of the intensity and spectral index distribution of source F. The peculiar overall Z-shaped morphology and the ultra steep spectrum of source F have been noted by Bridle et al. (1979) who designated the three separate components F1, F2, and F3. The higher resolution data reveal that (1) the central region of source F (F2) is a shell-shaped region and (2) the spectral index of the source flattens at the eastern source extremity.

#### 3.3.1. *The Halo "G" and "H"*

Possibly the most remarkable structure is seen in the northern part of the cluster: the "G" and "H" halo (e.g., Fig. 10). The crosses in Figure 10 are galaxies from the list of Fabricant

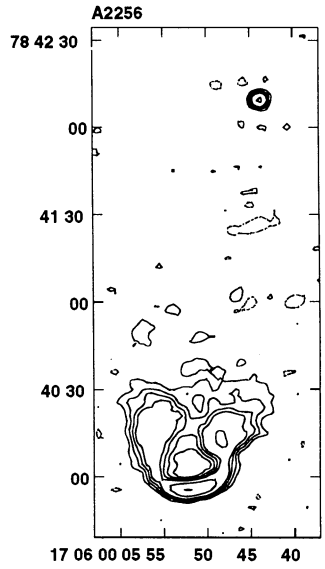


FIG. 4.—Source B on map 20B. The contours are at 40 × (−3, 3, 6, 9, 12, 24, 48, 96, 192, 384) μJy beam$^{-1}$.

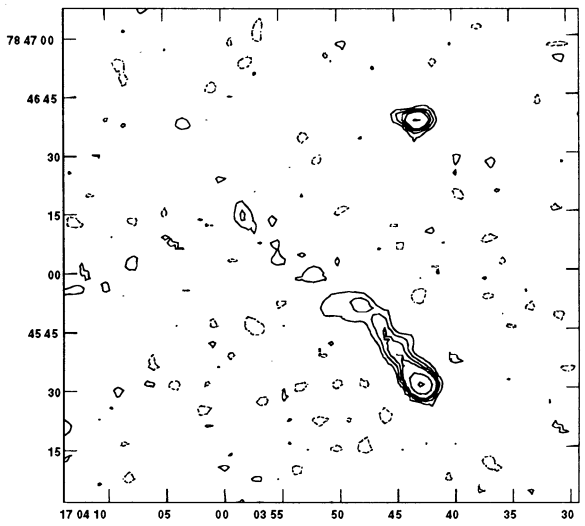


FIG. 5.—Source I on map 20B. The contours are at 30 × (−3, 3, 6, 9, 12, 24, 48, 96, 192, 384) μJy beam$^{-1}$.

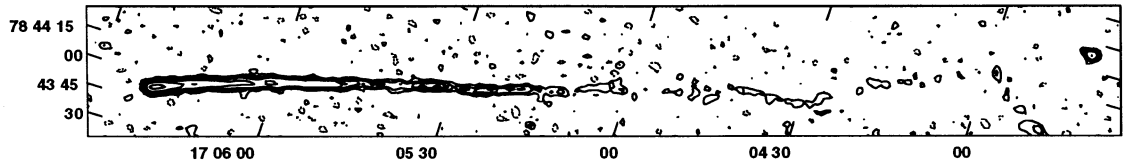


FIG. 6.—Source C on map 20B rotated over −18°. The contours are at 30 × (−3, 3, 6, 9, 12, 24, 48, 96, 192, 384) μJy beam$^{-1}$.

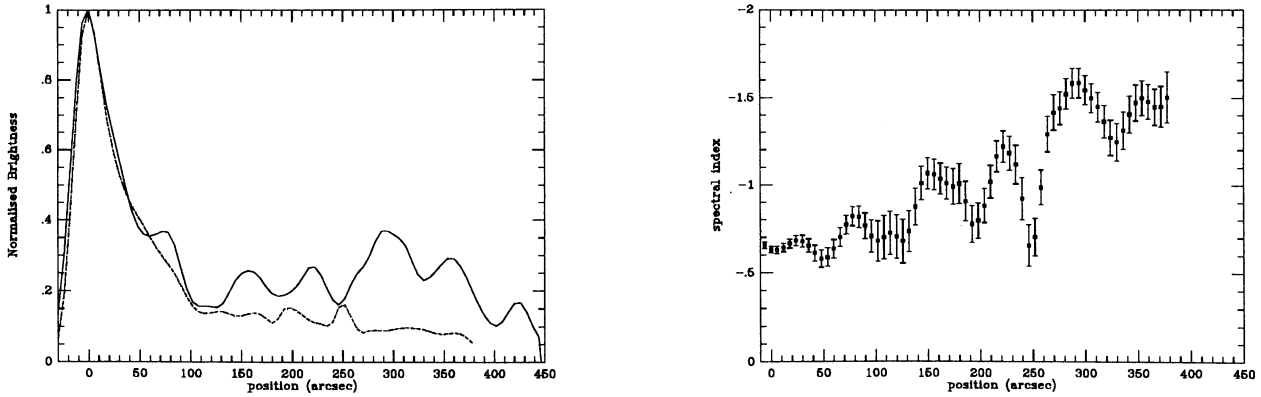


FIG. 7.—*Left*: Normalized peak of the brightness along the tail of source C on 90B map (*solid line*) and on 20CD map (*dashed line*). *Right*: Spectral index from the combined 20 and 90 cm data, along the tail of source C.

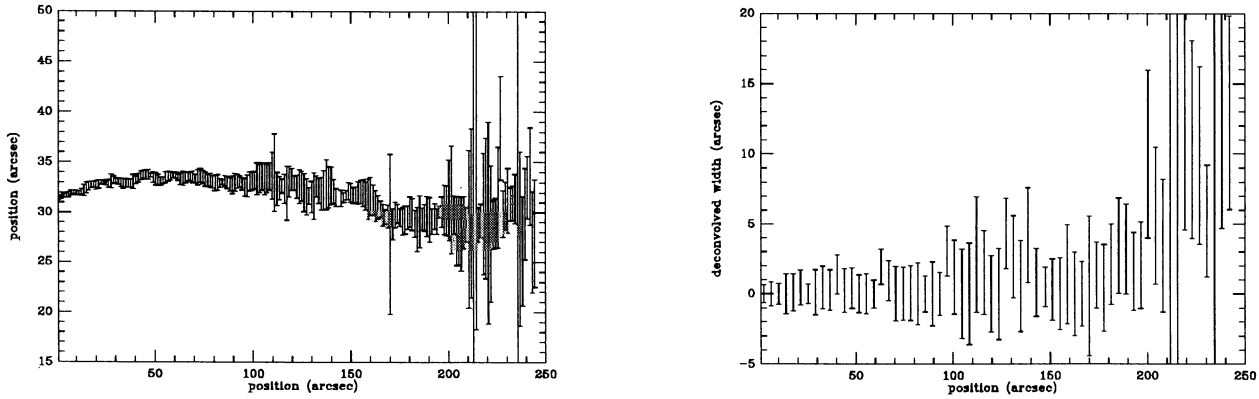


FIG. 8.—*Left*: The relative transverse position of the peak of the emission of the tail of source C after a rotation over −18°. *Right*: The deconvolved width (using quadratic subtraction with the convolving beam) of source C along the tail.

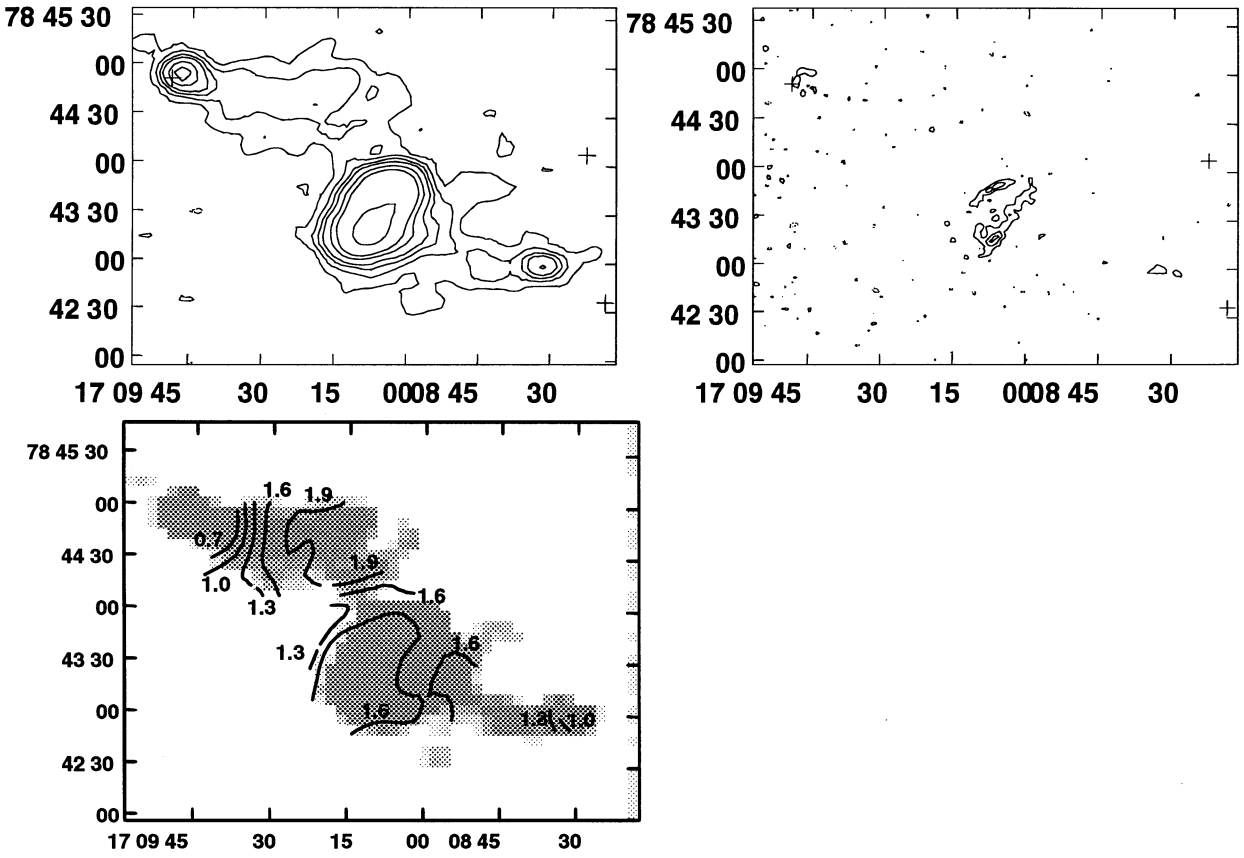


FIG. 9.—*Top left*: Source F on map 20CD. The contours are at 50 × (−3, 3, 6, 9, 12, 24, 48, 96, 192) μJy beam$^{-1}$. *Top right*: Source F on map 20B. The contours are at 50 × (−3, 3, 6, 9, 12, 24, 48, 96, 192) μJy beam$^{-1}$. *Bottom*: The spectral index distribution of source F at 25″ resolution, from a combination of the 20CD map and the 90B map, only including points brighter than 0.3 mJy beam$^{-1}$ and 1.5 mJy beam$^{-1}$, respectively. The contours are labeled in the map and are superposed on a gray-scale representation of the 20CD map.

et al. (1989) for which spectroscopic measurements indicate that they are not foreground or background galaxies, but members of the cluster.

The G and H halo should not be confused with the second extended (> 10′) region centered at source D that is marginally detected in the Westerbork 608 MHz maps. The maps presented in this paper do not have the sensitivity to detect this large region.

In addition to the Westerbork maps, the 20CD map shows the following remarkable features of the G and H halo (e.g., Fig. 10). First, the whole region seems to have well-defined boundaries; the edge in the southeast being particularly sharp. Second, filamentary structure is seen at several places. There are four or five filaments projecting outwards from the brightest region above source C. Third, there are bright spots in the region G and north of the tail of source C. The peak of the brightest spot of the region G is at $17^h06^m50^s.7$, 78°48′40″.7 and coincides with the galaxy at $17^h06^m50^s.5$, 78°48′39″. The bright spot north of source C is at $17^h05^m23^s.606$, 78°46′36″.00. The cluster galaxy at the position $17^h05^m24^s.1$, 78°47′06″ is located too far from the radio source to be accepted as a certain identification. Fourth, at higher resolution (<4″) the halo is completely resolved, indicating that it does not contain compact structures on these or smaller scales.

### 3.3.2. *Additional Extended Sources*

In Figure 11 we present maps of additional extended sources. Source D has a cluster galaxy situated between the two "lobes." The radio source has a classical double morphology (e.g., Miley 1980).

Although some of the other extended sources may be head-tail galaxies we cannot make such a classification without definite optical identification with a galaxy in the cluster. The background source counts at 1400 MHz (e.g., Katgert, Oort, & Windhorst 1988) indicate that 20–30 sources to the limit of 1 mJy are expected in the 22′.5 region around the pointing center. It is therefore likely that some of the extended sources are not located in the cluster, but are powerful radio sources at larger distances.

## 4. DISCUSSION

### 4.1. *Comparison with X-Rays*

Recently Abell 2256 was observed using the imaging proportional counter (PSPC) on board the *ROSAT* X-ray satellite. The X-ray morphology was observed to be double and interpreted as an indication that Abell 2256 is a merger of a small and large cluster (Briel et al. 1991; Henry & Briel 1991; Davis & Mushotzky 1993). In Figure 12 we present an overlay of the X-ray data from Briel et al. (1991) with the 20CD map.

We shall next discuss possible morphological correspondences between the X-ray and the radio emission and compare the pressures in the hot X-ray gas with the equipartition pressures that can be calculated for the radio plasma.

#### 4.1.1. *Morphology*

Although the spatial resolution of the X-ray map (48″) is considerably poorer than that of the radio map, several points

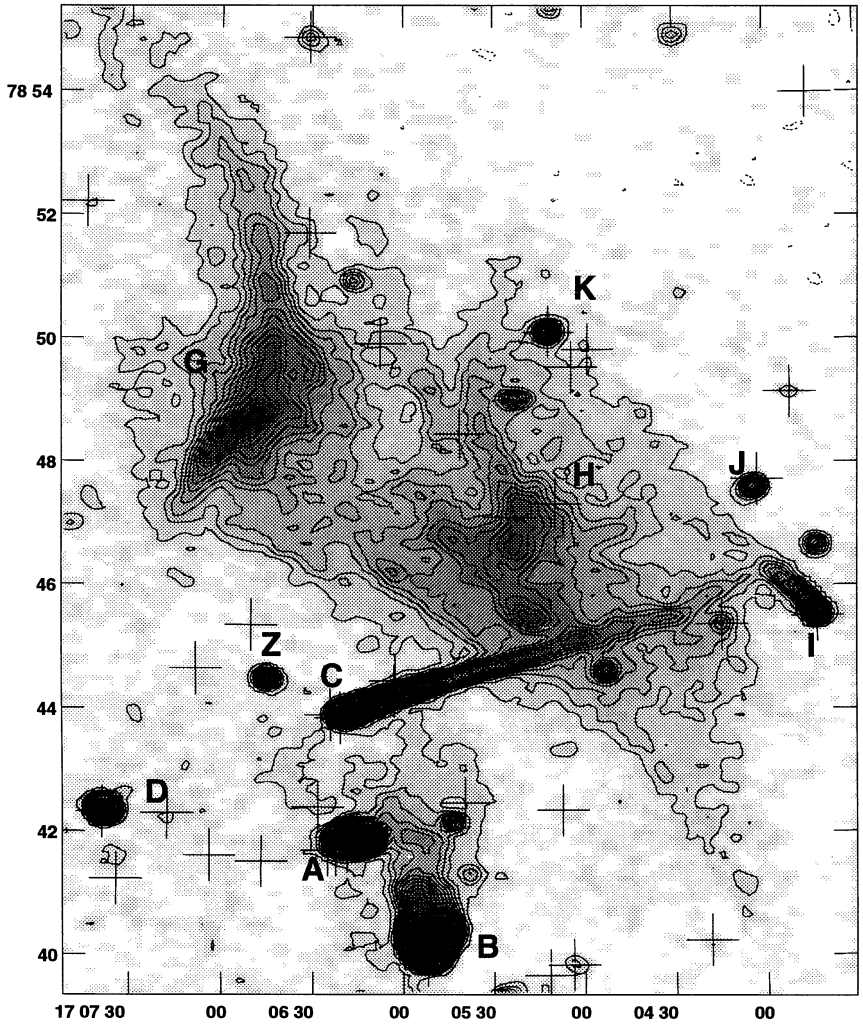


FIG. 10.—Part of the 20CD map that shows the central region with the G and H halo

of comparison are worth noting. First, the X-ray contours clearly follow the northwest edge of the diffuse radio emission. Second, this diffuse radio emission is located northwest of the two merging clusters. Third, none of the head-tails listed in Table 3 coincides with a peak in the X-ray map. Fourth, the three head-tails A, B, and C are located at a distance $\lesssim 1.5$ from the center of the presumed merging subcluster.

#### 4.1.2. *Pressures*

The *ROSAT* observations allow us to compare the equipartition pressures determined from the radio observations with the thermal pressures in the X-ray gas.

In the calculations of the equipartition value for the pressure and the magnetic filed of the relativistic gas we assumed a low-frequency cutoff of $10^7$ Hz, a high-frequency cutoff of $10^{11}$ Hz, equal to energy density in protons and electrons, a filling factor of 1, and cylindrical symmetry of the emitting regions (e.g., Miley 1980). In Table 4 the results for the sources with an optical identification and that are detected at 90 cm are given. Column (2) gives the volume used for the calculations and column (5) the projected distance to the center of the cluster. The values for the equipartition magnetic field and the pressures (cols. [3] and [4], respectively) are in good agreement with those found by Bridle et al. (1979).

*ROSAT* found clear evidence for substructure in the hot gas associated with Abell 2256 (Briel et al. 1991). Briel et al. fitted modified isothermal King profiles to the X-ray surface brightness, one to the main body of the cluster, and one to a secondary peak—supposedly a poor cluster in the process of merging with the main cluster.

TABLE 4

EQUIPARTITION PRESSURE AND MAGNETIC FIELDS FOR RADIO SOURCES IN ABELL 2256

| Source (1) | Volume ($kpc^3$) (2) | Magnetic Field ($\mu G$) (3) | Pressure ($10^{-12}$ dyn $cm^{-2}$) (4) | Projected Distance (5) |
|---|---|---|---|---|
| A | $5.9 \times 10^3$ | 7.5 | 3.25 | 1.6 |
| B | $2.9 \times 10^6$ | 1.2 | 0.09 | 3.5 |
| C | $2.5 \times 10^3$ | 9.3 | 5.00 | 2.4 |
| D | $3.8 \times 10^2$ | 7.5 | 3.19 | 2.4 |
| E | $1.8 \times 10^2$ | 7.5 | 3.24 | 13.8 |
| F3 | $1.4 \times 10^6$ | 1.3 | 0.09 | 9.1 |
| G | $2.7 \times 10^7$ | 0.6 | 0.02 | 6.5 |
| I | $9.0 \times 10^2$ | 7.5 | 3.22 | 9.7 |
| K | $5.9 \times 10^2$ | 6.4 | 1.22 | 9.2 |
| AD | $1.5 \times 10^4$ | 2.0 | 0.22 | 19.1 |

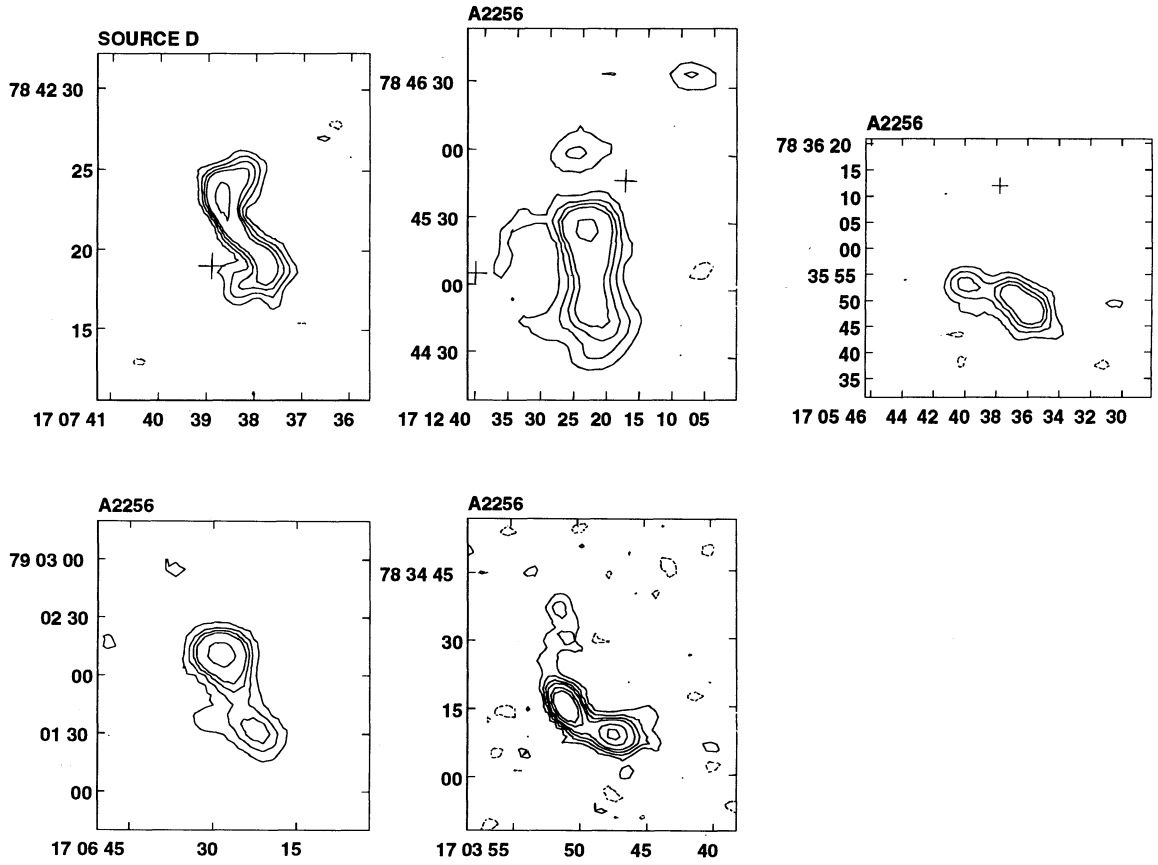


FIG. 11.—*Top left*: Source D on map 20A. The contours are at 50 × (−6, −3, 3, 6, 9, 12, 24, 48, 96, 184) μJy beam$^{-1}$. *Top center*: Source M on map 20CD. The contours are at 30 × (−3, 3, 6, 9, 12, 24, 48, 96, 192, 384) μJy beam$^{-1}$. *Top right and bottom right*: Sources L and P on map 20B. The contours are at 50 × (−3, 3, 6, 9, 12, 24, 50, 100) μJy beam$^{-1}$. *Bottom left*: Source T on map 20CD. The contours are at 100 × (−3, 3, 6, 9, 12, 24, 50, 100) μJy beam$^{-1}$.

The density $n$ as function of the distance from the cluster center $r$ can be described by deprojected King profiles (e.g., Forman, Jones, & Tucker 1985):

$$n(r) = n(0)\left(1 + \frac{r^2}{r_c^2}\right)^{-3\beta/2}, \quad (1)$$

where $n(0)$ is the central density, $r_c$ is the core radius, and $\beta$ the density slope parameter. The central density $n(0)$ was found using (1) the X-ray counts to luminosity factor as given by Briel et al. (1991), and (2) the emissivity $\epsilon$ normalized by the electron density squared ($n_e^2$) as a function of temperature and *ROSAT* bandwidth (0.1–2.4 keV) as estimated from the figures of Mewe, Gronenschild, & van den Oord (1985). Note that this value for the normalized emissivity differs only marginally from that determined using the old prescription of Blumenthal & Tucker (1974). The central pressure was subsequently found assuming a perfect gas law. The parameters of the X-ray–emitting gas in the two components are summarized in Table 5. The core radius $r_c$, the density slope $\beta$, and the temperature $T$ are taken from Briel et al. (1991). The central electron density for the main cluster is similar to that found by Fabicant et al. (1989).

In Figure 13 we show the pressure in the X-ray gas for the main cluster (left) and for the sub cluster (right ) as a function of the distance from the respective centers. In Figure 13 the equipartition pressures in the radio plasmas for the source of Table 4 are also given.

The calculated equipartition pressure for the radio plasma is systematically lower than the pressure in the X-ray gas for distances from the main cluster center of less than 1 Mpc. Although unlikely, it is possible that the radio sources are located far from the cluster center in a region where the pressures from the X-ray–emitting gas is closer to that deduced from the radio plasma. The results of Feretti et al. (1990) also indicate that the equipartition pressure of the radio sources in their sample of four clusters is systematically lower than the corresponding thermal pressures of X-ray gas that surrounds the radio sources. This holds for both the jets and the lower brightness regions in these four clusters.

It is likely that the difference is due to the numerous assumptions that are used in calculating the equipartition pressure. These are various ways in which these assumptions can be relaxed so as to increase the pressure to equal the X-ray pressure (e.g., Feretti et al. 1990). The equipartition pressure increases with a factor of 10 if (1) the filling factor of the radiating relativistic plasma is lower from 1 to 0.02 (low filling factors have been suggested for the lobes of Cygnus A; Bridle

TABLE 5

PROPERTIES IF THE X-RAY–EMITTING GAS

| $r_c$ (kpc) | $\beta$ | $T$ (keV) | $\epsilon/n_e^2$ (ergs cm$^3$ s$^{-1}$) | $n(0)$ (cm$^{-3}$) | $P(0)$ (dyn cm$^{-2}$) |
|---|---|---|---|---|---|
| 483..... | 0.756 | 10.3 | $1 \times 10^{-23}$ | 0.0021 | $3.5 \times 10^{-11}$ |
| 430..... | 1.1 | 2.0 | $9.2 \times 10^{-24}$ | 0.0024 | $6.3 \times 10^{-12}$ |

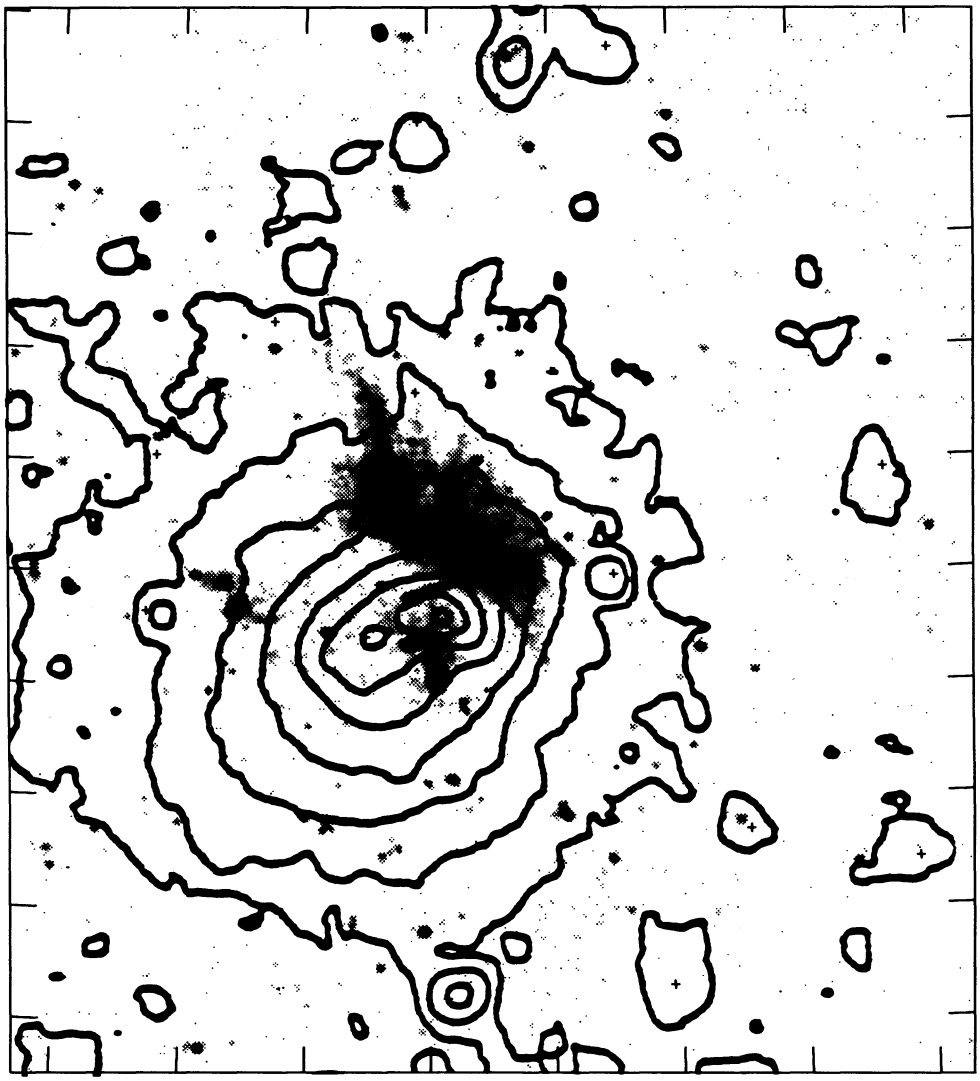

FIG. 12.—Contour map of the X-ray brightness distribution taken from an X-ray image of Henry & Briel (1991). The contours are at 1.25, 2.5, 5.0, 9.0, 17.0, 28.0, 39.0, 46.0 PSPC counts per 16 × 16 arcsec$^2$. The gray-scale representation is of the 20CD radio map at 1465 MHz (see Fig. 1).

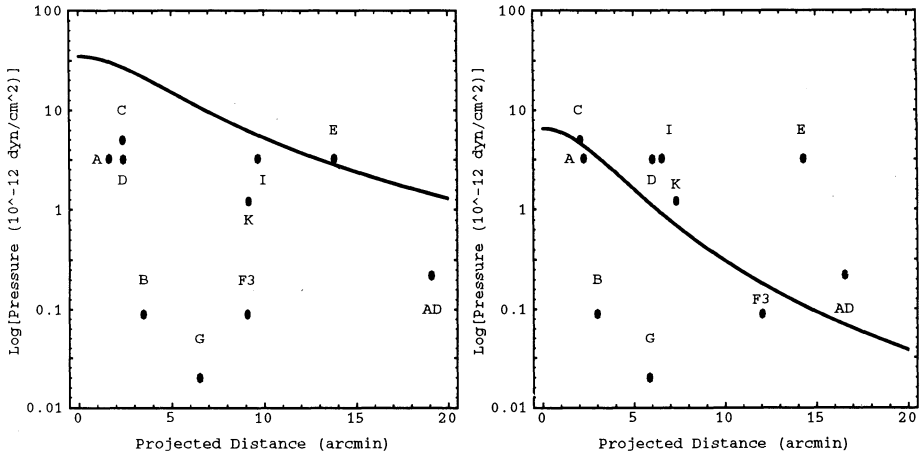


FIG. 13.—Pressure in the X-ray–emitting gas for the main cluster (*left*) and for the subcluster (*right*) as function of the distance from the respective centers. The equipartition pressures in the radioplasma for the sources are also given.

& Perley 1984), (2) the energy ratio between heavy particles and electrons values is $\sim 50$, or (3) the low-frequency limit is 1 kHz. Furthermore, it is possible (4) to assume the presence of another pressure component, such as entrained thermal gas or (5) to assume a departure from equipartition.

Although the uncertainty in the equipartition pressure is considerable, the conclusion that the radio sources are at least partially confined by the X-ray gas is probably correct. A similar conclusion was reached by Bridle et al. (1979) using older X-ray data of Mushotzky et al. (1978).

This means that large-scale motion (e.g., large-scale turbulence) in the X-ray gas will have a profound influence on the morphology of the radio sources. It also indicates that the morphology of the more relaxed radio structure (such as G and H) can in principle be used to constrain the estimates on any small- and large-scale turbulence in the hot X-ray gas.

### 4.2. *Nature of the Halo Arcs*

Most striking in the VLA maps is the diffuse region in the north of the cluster encompassed by features G and H (e.g., Fig. 10). The results from the old Westerbork maps for this region can be summarized as follows:

1. The extent of the region is remarkably large, estimated to be 1.0 by 0.3 Mpc.
2. It has a uniform spectral index of $0.8 \pm 0.1$ (see also Haslam et al. 1978).
3. The percentage polarization is uniform with an average value of 20%.
4. The alignment of the electric vectors suggests a well-ordered magnetic field. The curvature of the electric vector follows the curvature of ridges of maximum brightness.

Our 20 cm VLA maps show the following additional features:

5. Sharp edges.
6. Possible filamentary structure.
7. Brighter spots in region G and H of which at least one is identified with a cluster galaxy.

The possibility that the features G and H are located in our own Galaxy was rejected by Bridle et al. (1979) on the basis of its high galactic latitude and the very low possibility that a feature like this would lie in front of a cluster. Since the VLA observations show that the northwest edge of the halo follows the X-ray contours suggesting a physical connection between the two plasmas, the conclusion is reinforced that the features G and H are indeed connected with the cluster.

Bridle et al. (1979) suggested two possible interpretations for this extended region. First, the features G and H could be a single wide-tailed source whose "head" is either unrecognizable or possibly source K. The morphology as seen in our higher resolution data does not favor this interpretation. There is no clear sign of a connection between the source K and the brighter spots in the G and H halo. Furthermore, the other characteristics such as the uniform spectral index and the polarization structure are difficult to understand in this interpretation. Second, region H might be produced by leakage of particles from source C. As Bridle et al. (1979) note, this is difficult to understand, since the spectrum of H is flatter (younger emitting electrons) than the tail of C. Our high-resolution data on source C indicate that source C is an extremely long head-tail galaxy extending as far as the head-tail source I. At our high resolution no morphological connection to the extended region is apparent.

The favored interpretation of the *ROSAT* X-ray of Abell 2256 data is that we are witnessing a small and a large cluster merging (Briel et al. 1991). Fabian & Daines (1991) suggested that the galaxies A, B, and C are probably members of the merging subcluster and that stripping of the subcluster gas may have created the diffuse radio sources from their lobes. This supposed origin of the diffuse emission is unsupported by our high-resolution VLA data which show no structures, such as diffuse bridges of emission connecting the head-tail galaxies with the radio halo that would be expected in such scenario. Furthermore the relatively flat spectral index of the halo as compared to the steeper spectral index characteristics of radio tails argues against this interpretation.

In secondary electron models (Dennison 1980; Vestrand 1982) the relativistic electrons are supposed to originate from the collisions of relativistic protons with thermal protons in the X-ray gas. Since from the *ROSAT* data this radio halo does not coincide with the X-ray halo (e.g., the densest region), this process seems unlikely to be the dominant one in producing the radio halo.

Models of radio halos invoking in situ acceleration by turbulence seems attractive since they could readily explain the relatively flat spectral index in the Abell 2256 halo. One possible origin for the turbulence is the wake of cluster galaxies (Roland 1981). However, the fact that there is no apparent excess of galaxies in the region of this radio halo is an argument against such turbulent wake models. Furthermore, models of Goldman & Rephaeli (1991) and de Young (1992) show that galactic wakes are inadequate to produce the observed halos (see also Tribble 1993). A more likely source of turbulence might be the merging of the clusters (e.g., Edge, Steward, & Fabian 1992 and Watt et al. 1992). Could the halo emission be a by-product of this event? In this case, we would expect to see radio emission from regions that contain shocked material. Numerical hydro/$N$-body simulations of merging clusters suggests that a strong central shock is expected between the merging clusters and perpendicular to the merger axis (Roettiger, Burns, & Loken 1993). Since this supposed geometry is not seen (e.g., Fig. 12), we regard turbulent acceleration by the merger of the cluster as unlikely to be the dominant mechanism that produces the this halo.

It is interesting to note that galaxies coincide with several of the bright maxima in the radio halo. We therefore suggest that the region contains two or three head-tail galaxies that are strongly disturbed by the large-scale turbulence and shear caused by the infall of the subcluster. In such a scenario we have to consider the energy of the emitting synchrotron plasma. We have calculated the minimum energy content $U_{\rm min}$ of the G and H halo, using the assumptions outlined in § 4.1.2 and find $U_{\rm min} = 6 \times 10^{58}$ ergs. Since the minimum energy of the head-tail galaxy B is $U_{\rm min} = 5 \times 10^{57}$ ergs, it is possible that a few head-tail galaxies with energies comparable to source B can provide the energy to power the G and H halo. A second requirement is about the timescale within which the radio plasma must have been distributed over the area of the present H and G region. Synchrotron-emitting particles with an initial power-law spectrum will show a break in the spectrum after

$$t_{\rm br} \sim 0.82 B^{1/2} (B^2 + B_R^2)^{-1} (1 + z)^{-1/2} \nu_{\rm br}^{-1} \ [\rm yr] ,$$

where $B$ is the source magnetic field in Gauss, $B_R = 4 \times 10^{-6} (1 + z)^2$ is the equivalent magnetic field strength of the microwave background in Gauss, and $\nu_{\rm br}$ is the frequency in GHz at

the break (e.g., Miley 1980). To be able to determine the location of the break for the H and G halo additional radio maps at higher frequencies are required. However, the central area has a fairly normal spectral index of $0.8 \pm 0.1$ between 610 and 1400 MHz with hints of steeper indices in the outer regions (Bridle et al. 1979). This indicates that a spectral break occurs at a frequency $>1400$ MHz, yielding $t_{\rm br} < 2.3 \times 10^7$ yr. If the source magnetic field originates in head-tail galaxies that have typical magnetic fields of 5 $\mu$G the magnetic field of the H and G halo will have been substantially stronger in the past. This however does not significantly change the estimate of the upper limit to $t_{\rm br}$, since the estimte is largely determined by the equivalent magnetic field strength of the microwave background.

If we adopt a source lifetime of $3 \times 10^7$ yr, then the radio plasma from the assumed head-tails have been distributed over the area of the H and G halo over a timescale of a few times $10^7$ yr. Whether this is a sufficient long period of time depends on (1) the initial extent of the head-tails and (2) the velocity with which the synchrotron-emitting plasma is transported throughout the cluster. The initial extent of the radio sources before diffusing out is not known. If we assme that the region contained a few radio sources with an initial size of a few hundred kiloparsecs, then to fill the H and G area, relativistic electrons will have to travel over distances of order 50–100 kpc within a few times $10^7$ yr implying velocities of order 1500–3000 km s$^{-1}$.

The Alvén speed for the magnetic field of the G and H halo ($B_{\rm min} \sim 0.5$ $\mu$G) and for the head-tails ($B_{\rm min} \sim 5$ $\mu$G) is 35 and 350 km s$^{-1}$, respectively, using the number density in the halo from the *ROSAT* X-ray measurements of 0.001 cm$^{-3}$. If the speed at which the electrons can diffuse is limited by the Alfvén speed, the extent of the H and G radio halo is difficult to understand (see, however, Holman, Ionson, & Scott 1979). Briel et al. (1991) suggested that the two merging clusters are colliding with a velocity of order 2000 km s$^{-1}$. If this is indeed the case, the merger would drag relativistic plasma of the initial head-tails with it, giving the region the shape it has now.

Studying polarization and Faraday rotation of radio sources, in the centers of clusters yields information on both the cluster magnetic field and the hot gas (e.g., Garrington, Conway, & Leahy 1991; Perley & Taylor 1991; Tribble 1991 and Jing Ping Ge & Owen 1993). Since we only have information on the polarization and not on the rotation measure of the H and G halo, the information on the cluster magnetic field and the hot gas from the radio data is rather limited. It is, however, remarkable that the percentage of the polarization at 1400 MHz of the H and G halo is large (20%). In a sample of radio sources of 47 double radio sources with one-sided jets studied by Garrington et al. (1991) none of the sources has a percentage polarization at 1400 MHz as large as the H and G halo. The best-studied radio halo is the halo in the Coma cluster which has no detected polarization to a limit of 1% in the center at a resolution of $\sim$40 kpc (Kim et al. 1990). Following Garrington et al. (1991), we define the Faraday depth:

$$\phi = \int n B_z \, dl \, ,$$

where $n$ is the thermal electron density, $B_z$ the longitudinal magnetic field, and $dl$ the infinitesimal path length along the line of sight. We assume a Gaussian distribution for $F(\phi)$ with standard deviation $\Delta$. The depolarization DP between two wavelengths $\lambda_1 > \lambda_2$ is then

$$\Delta \sim \left( \frac{-\ln DP}{\lambda_1^4 - \lambda_2^4} \right)^{1/2}$$

(but see Tribble 1991 for a more elaborated expression). Naively we might expect that in a high-density and merging cluster such as Abell 2256, $\Delta$ will be relatively high, leading to relatively low polarization at 20 cm. However, the polarization is high. We will need more polarization data at different frequencies to address this problem properly. Since there is a clear connection between the morphology of the X-ray emission and the emission from the radio halo, it seems unlikely that the halo is located at the front of the cluster leading to a low Faraday depth and low $\Delta$. We suggest that the following might play a role: (1) the cluster magnetic field is relatively low, giving a low value for $\Delta$ or (2) the reshaping of the head-tails during the merging led to a relatively ordered magnetic field in the G and H halo, therefore a high polarization.

### 4.3. *The Tail of Source C*

If source C is a head-tail galaxy, its length (425″, corresponding to 700 kpc) classifies it among the longest head-tail sources known. Summarizing the properties of source C:

1. The peak of the emission coincides with a magnitude 15.3 optical galaxy.
2. The brightness decreases rapidly with distance from the head (e.g., Fig. 8).
3. The radio spectrum steepens away from the galaxy (Bridle et al. 1979).
4. The tail does not seem to be morphologically connected to the northern diffuse emission.
5. The tail has a length of 700 kpc. It is slightly curved and there is a kink at a distance of 570 kpc from the peak.
6. Its width is less than 2.5 kpc (e.g., unresolved at 20 cm VLA A configuration) and does not significantly widen between the head of the source and the end of the tail (e.g., Fig. 8).

These extreme properties call for a reconsideration of the nature of the object.

Independent of their environment, most radio sources are now known to possess jetlike features in their morphologies that are believed to be channels along which energy is transmitted from the nucleus to the lobes of the radio sources (Blandford & Rees 1974). These jets are supposed to be produced by intrinsic effects within the nuclei of the radio galaxies and are distinguished from "tails" whose morphologies are presumed to be governed by environmental effects (e.g., Miley 1980). Could the straight narrow structure in source C be a one-sided jet instead of a tail?

Bridle & Perley (1984) define a "jet" as a feature on a radio map that is (1) at least four times as long as wide, (2) separable from other extended structure, and (3) aligned with a compact radio core. Source C clearly satisfies the first two criteria. The third criterion is not satisfied. The radio map does not show a clear nuclear component separated from the "jet." A further characteristic that distinguish source C from jets are that most jets in sources with powers $\lesssim 10^{24.5}$ W Hz$^{-1}$ are two sided, whereas the low-power source C is one sided with no sign of a counterjet. Given the additional fact that source C occurs in close proximity to so many head-tail galaxies, we favor its interpretation as an extreme narrow angle tailed galaxy.

Assuming that source C is a indeed a head-tail, its extreme morphology might provide constraints on the physics of jets as well as the conditions of the intracluster medium around source C. Within the context of the standard model of narrow angle tails (NATs), the properties of source C that should be explained are its small width, its length, and its straightness. NAT sources with large integrated radio powers tend to be longer (O'Dea & Owen 1985b). The power of source C is, however, not extreme and does not give a clue to its extreme length. Given this extreme length, it would be surprising if both the source and its velocity vector were not closely perpendicular to the line of sight. If the souce were aligned close to the line of sight its true (deprojected) size would be staggering.

If we assume that the radio emission from source C traces the trajectory of the associated galaxy, we can attempt to estimate the velocity of the galaxy along this trajectory. The cluster potential that determines the orbit of the galaxy can be obtained from the X-ray data. We will use the potential as determined by Fabricant et al. (1989) from *Einstein* data.

An orbit through this fixed potential is completely determined if six parameters are known at a given time: the three components of the velocity vector and the three components of the position vector.

Consider the initial situation when the galaxy associated with the radio emission was at the beginning of the present tail, that is, close to source I (e.g., Figs. 6 and 8). Four of the six parameters characterizing the orbit are determined, namely, the projected position (e.g., $\alpha$ and $\delta$), the projected direction of the velocity at the beginning of the tail, and the line-of-sight velocity of the galaxy at its present location. The two parameters that are unknown are the projected velocity in the direction of the jet, the position and velocity of the galaxy in the cluster along the line of sight.

In Figure 14 we show the trajectories for different initial velocities and distances out of the plane through the cluster center and perpendicular to the line of sight. From this we see that to explain the present position of the galaxy would require an initial velocity of 3500 to 2000 km $s^{-1}$. If the velocity of the galaxy were significantly less than 2000 km $s^{-1}$, the trajectory would be more curved towards the center and if the velocity of the galaxy were significantly more than 3500 km $s^{-1}$ the observed curvature would be less.

This basic conclusion requires that the source's initial location had a distance out of the plane through the cluster center and perpendicular to the line of sight of less than 0.5 Mpc. If the tail was located further out of this plane (e.g., >0.5 Mpc), its length would be even more extreme.

This simple model suggests that the velocity with which this head-tail moves through the cluster is 2–3 times larger than radial velocity dispersion as measured for the galaxies in this cluster.

Baan & McKee (1985) have modeled the morphologies of three well-observed head-tail galaxies by assuming that the bending of the beams is due to the ram pressure of the ICM inflow. We shall now apply a similar analysis to source C. For a galaxy that (1) moves perpendicular to the ejection direction of the jets and (2) has its jets ejected in the plane of the sky, their simple ram pressure model gives for the shape of the beam:

$$y = \frac{\cosh^{-1}(\alpha_s x + 1)}{\alpha_s}, \qquad (2)$$

where $y$ is the axis along the direction of the motion of the galaxy, $x$ is the axis perpendicular to the $y$-axis in the plane of

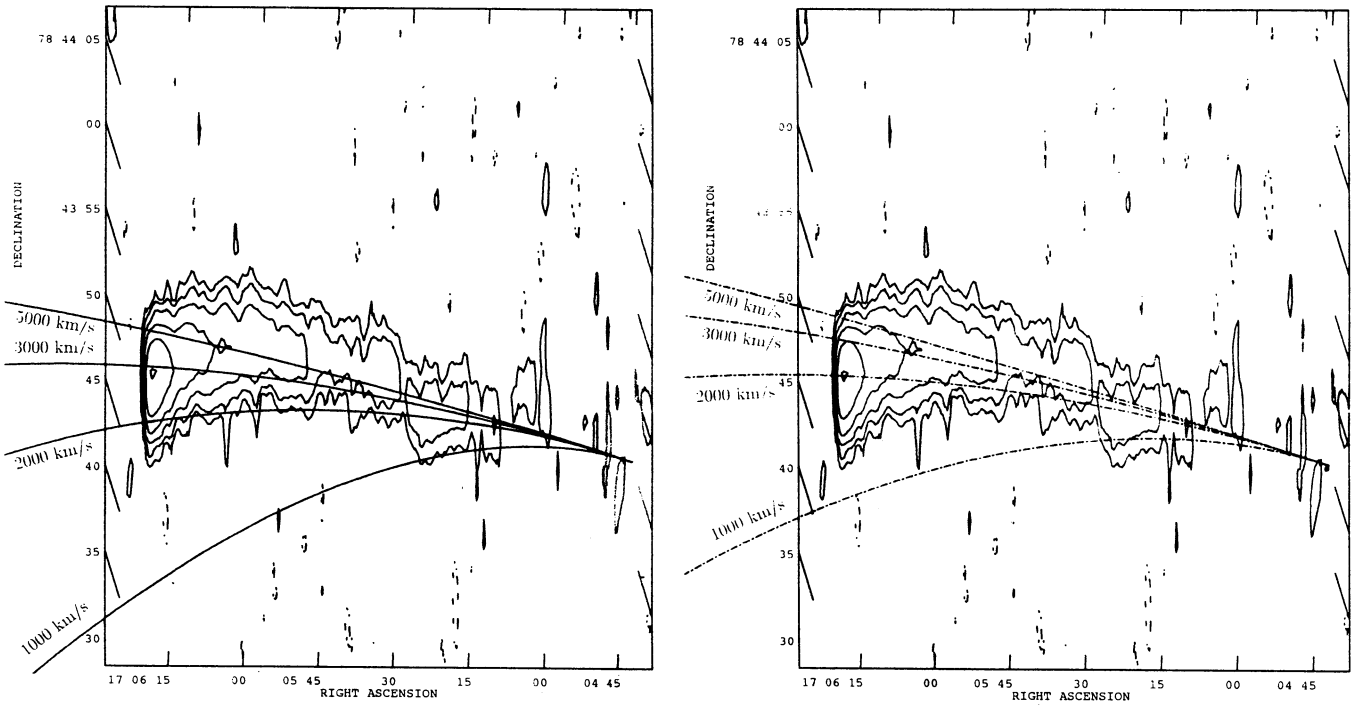


FIG. 14.—Trajectories for initial velocities of 1000, 2000, 3000, and 5000 km $s^{-1}$ and initial positions in the plane of the cluster (*left*) and at 500 kpc from the plane of the cluster center (*right*). The image is rotated over −18°, and the declination axis is stretched by a factor of 10.

the two jets, and $\alpha_s$ is a scaling factor:

$$\alpha_s = \frac{\rho_a}{\rho_j}\frac{c_d}{\pi r_b}\frac{V_g^2}{V_j^2}, \quad (3)$$

where $\rho_a$ is the ambient density, $\rho_j$ is the jet density, $c_d$ is the drag coefficient commonly used in fluid dynamics, $r_b$ is the beam radius, $V_g$ the velocity of the galaxy, and $V_j$ the velocity of the jet.

Since the jets are unresolved we cannot solve for the shape of the beams. For the supposed choice of geometry we can, however, estimate $\alpha_s$. If we assume that the jets must have been swept back within $y \sim 2$ kpc to a distance less than $x \sim 2$ kpc or to a distance less than $x \sim 250$ kpc, then from equation (2) we get $\alpha \sim 1$ or $\alpha \sim 2.5$, respectively. Those values are a magnitude larger than those that Baan & McKee (1985) found for the three well-resolved head-tail galaxies. If this head-tail has a velocity 2–3 times larger than the galaxies from Baan & McKee (1985) then a large $\alpha_s$ is expected.

Unfortunately, not enough is known about the jet characteristics to estimate a priori the scale factor $\alpha_s$. Apart from the intrinsic properties of the beam, external factors which might produce abrupt bending of the jets are (1) a large galaxy velocity (large $V_g$) and (2) a highly dense medium (a large $\rho_a$). As has been noted by Bridle et al. (1979), the bivariate radio luminosity function (RLF) of Abell 2256 does not differ significantly with the standard RLF of Auriemma et al. (1977). This is consistent with the suggestion that the remarkably fast bending does not have to be associated with anomalous intrinsic properties of the galaxy, but with external properties such as high galaxy velocity and high ambient density.

A necessary assumption in this model is that the scale height of the ISM is comparable or less than the bending scale of a few kpc. Otherwise the ICM cannot exert its ram pressure efficiently enough in order to obtain the small bending scale. The low percentage of spiral galaxies in Abell 2256 might be due to ram stripping of galaxies by the ICM. This process gives rise to the small scale height of the ISM in the galaxy that is associated with radio source C.

The small-scale straightness of some tails (e.g., 3C 129; Jaffe & Perola 1973) indicates that the medium is quiescent with turbulent velocities below 100 km s$^{-1}$, while the as yet unexplained sharp bends in others (Burns et al. 1986) suggest high-velocity, large-scale turbulence.

It is interesting to consider whether the extreme straightness of the source C provides information about possible turbulence in the X-ray gas in Abell 2256. If the equipartition pressure is close to the true pressure in the radio tail (see § 4.1.2) then the X-ray gas confines the radio gas. Subsequently, the tail will follow turbulent motions in the X-ray gas. If a transverse displacement $l_\perp$ over a scale length of $l_\parallel$ is caused by an individual eddy of size $(l_\parallel l_\perp)^{1/2}$, then the velocity $v_e$ of this eddy is

$$v_e = l_\perp / t, \quad (4)$$

where $t$ the timescale over which the eddy exerts its pressure.

This timescale will correspond to the lifetime of the radio source, estimated to be about $10^8$ yr. This is also the time needed to travel over 400 kpc with a velocity of 2000 km s$^{-1}$. Hence the straightness of the source ($l_\perp < 20$ kpc) implies turbulent velocities of $v_e < 200$ km s$^{-1}$.

Its remarkable that the H and G halo might be the result of large-scale turbulence, whereas the morphology of source C probably implies that it has traveled through a medium with low turbulence. This suggests that the orbit of source C lies outside the volume where the merging is taking place. If both the lifetime of the radio source is significantly less than $10^8$ yr and the velocity of the radio source is more than 2000 km s$^{-1}$, this problem is less severe. In this case the constraints on the turbulent velocity are less stringent.

### 4.4. *The General Picture*

One of the most fundamental questions posed by the observations of Abell 2256 is why its radio properties are so anomalous. An essential ingredient is the integral bivariate radio luminosity function (RLF) (Auriemma et al. 1977). Bridle et al. (1979) find that there is no significant difference between the RLF of Abell 2256 and the general RLF given by Auriemma et al. (1977). From this they conclude that the excess of head-tails should be attributed to the unusual properties of the cluster medium rather than to a peculiar galaxy content.

Head-tail sources are supposed to be produced when a radio galaxy moves at high speeds through a relatively dense intracluster medium. Source C is a prime example of a fast-moving source. Therefore the high velocity dispersion of the galaxies combined with the high density of the intracluster medium might explain the large number of head-tail galaxies.

We have suggested that the H and G radio halo in Abell 2256 is composed of a few head-tail galaxies whose radio morphologies have been distorted due to the merging of the subcluster. This would imply that the formation of this halo is directly linked to the large scale shear and turbulence in the cluster. In such a picture the origin of both the halo and the head-tail galaxies would be directly coupled to the large velocity dispersion of the cluster galaxies and to the infall of the subcluster.

It seems to be a general trend that clusters with a radio halo do not possess a cooling flow (e.g., Edge et al. 1992; Watt et al. 1992; Burns et al. 1992; Jaffe 1992). Several suggestions have been made to explain this anticorrelation. Burns et al. (1992) proposes that cooling flows suppresses the diffusion of turbulently amplified $B$-fields inhibiting the formation of radio halos. Tribble (1993) argues that this process is not efficient enough and that it is more likely that a cluster merger both stops the cooling flow as well as reaccelerates remnant relativistic particles leading to a radio halo. If the merger indeed distorts head-tails within the H and G region, particle reacceleration does not have to be the dominant mechanism producing this halo. The anticorrelation between cooling flows and radio halo can still be explained within the context of a merger model, at least in the case of A2256.

Despite extensive searches for radio halos (Jaffe & Rudnick 1979; Hanisch 1982a; Andernach et al. 1986), only about 10 are known. This might be because merging clusters that have a few head-tails near the merger region are rare.

Further characteristic properties of the clusters that are associated with radio halos are (e.g., Hanisch 1982b): (1) they have an unusually low content of spiral galaxies ($\sim$10%), (2) their galaxies have a large velocity dispersion ($\sim$1000 km s$^{-1}$), and (3) they have large X-ray luminosities ($L \sim 10^{44}$–$10^{45}$ ergs s$^{-1}$) and large X-ray core radii (>0.3 Mpc). These characteristics indeed suggests that merging is important for clusters with halos.

## 5. CONCLUSION

The complex radio emission from the rich X-ray cluster of galaxies Abell 2256 has been mapped at 20 cm using the VLA

in A, B, C, and D configurations and a 90 cm using the VLA in B configuration, giving detailed information on radio structures on scales up to 10′ with an unprecedented angular resolution of 1″.5.

We have shown that the northern radio halo of Abell 2256 has sharp edges and possible filamentary structure. We suggest that this halo is composed of a few head-tail galaxies that are heavily distorted due to the infalling subcluster inferred from the *ROSAT* data.

One galaxy has been observed to have a remarkably narrow, straight tail extending to at least about 700 kpc. From the small deviations of the remarkable straightness of this source, we estimate the turbulence in the confining X-ray gas around this source to be $\sim 200$ km s$^{-1}$ on scales of about 20 kpc.

The spectrum of ultrasteep source "F" appears to flatten at both extremities. If the identification of the eastern "flatter" region with a cluster galaxy is correct, source F is a head-tail galaxy with an extreme spectrum and a peculiar Z-shaped morphology.

The extreme radio properties, the large velocity dispersion of the cluster galaxies, and the high gas density inferred from the X-ray observations can all be understood within the merging subcluster model for Abell 2256.

It is a pleasure to thank Wil van Breugel, Andy Fabian, Alastair Edge, and Walter Jaffe for useful discussions and Peggy Perley and Dave Wunkler for help with the planning and reduction of the VLA observations.

## REFERENCES

Andernach, H., Sievers, A., Kus, A., & Schnaubelt, J. 1986, A&AS, 65, 561
Auriemma, C., Perola, G. C., Ekers, R., Fanti, R., Lari, C., Jaffe, W. J., & Ulrich, M. H. 1977, A&A, 57, 41
Baan, W., & McKee, M. 1985, A&A, 143, 136
Blandford, R. D., & Rees, M. J. 1974, MNRAS, 169, 395
Blumenthal, G. R., & Tucker, W. 1974, in X-Ray Astronomy, vol. 43, ed. R. Giacconi & H. Gursky (Dordrecht: Reidel), 99
Bothun, G., & Schombert, R. E. 1990, ApJ, 360, 436
Bridle, A., & Fomalont, E. 1976, A&A, 52, 107
Bridle, A., Fomalont, E., Miley, G., & Valentijn, E. 1979, A&A, 80, 201
Bridle, A. H., & Perley, R. A. 1984, ARA&A, 22, 319
Briel, U., et al. 1991, A&A, 246, L10
Burns, J., Sulkanen, M., Gisler, G., & Perley, R. 1992, ApJ, 388, L49
Burns, J. O., O'Dea, C., Gregory, S., & Balonek, T. 1986, ApJ, 307, 73
Butcher, H., & Oemler, A. J. 1978, ApJ, 226, 559
Cornwell, T. J., & Perley, R. A. 1992, A&A, 357, 261
Cornwell, T. J., & Wilkinson, P. N. 1981, MNRAS, 196, 1067
David, L. P., Slyz, A., Jones, C., Forman, W., Vrtilek, S. D., & Arnaud, K. A. 1993, ApJ, 412, 479
Davis, D. S., & Muschotzky, R. F. 1993, AJ, 105, 409
de Young, D. S. 1992, ApJ, 386, 464
Dennison, B. 1980, ApJ, 270, 410
Edge, A., Steward, G. C., & Fabian, A. C. 1992, MNRAS, 258, 177
Faber, S., & Dressler, A. 1977, ApJ, 82, 187
Fabian, A., & Daines, S. 1991, MNRAS, 252, 17P
Fabricant, D., Kent, S., & Kurtz, M. 1989, ApJ, 336, 77
Feretti, L., Spazzoli, O., Gioia, I., Giovannini, G., & Gregorini, L. 1990, A&A, 233, 325
Forman, W., & Jones, C. 1982, ARA&A, 20, 547
Forman, W., Jones, C., & Tucker, W. 1985, ApJ, 293, 102
Garrington, S., & Conway, R. 1991, MNRAS, 250, 198
Garrington, S., Conway, R., & Leahy, J. P. 1991, MNRAS, 250, 171
Goldman, I., & Rephaeli, Y. 1991, ApJ, 380, 344
Hanisch, R. J. 1982a, A&A, 111, 97
———. 1982b, A&A, 116, 137
Haslam, C., Kronberg, P., Walthausen, H., Wielebinski, R., & Schallwich, D. 1978, A&AS, 31, 99
Henry, J., & Briel, U. 1991, A&A, 246, L14
Holman, G., Ionson, J., & Scott, J. 1979, ApJ, 228, 576
Jaffe, W. J. 1992, in Clusters And Superclusters of Galaxies, ed. A. C. Fabian (Dordrecht: Kluwer), 109
Jaffe, W. J., & Perola, G. C. 1973, A&A, 26, 423
Jaffe, W. J., & Rudnick, L. 1979, ApJ, 233, 453
Jägers, W. J. 1986, Ph.D. thesis, Univ. Leiden
Jing Ping Gee & Owen, F. N. 1993, AJ, 105, 778
Katgert, P., Oort, M. J. A., & Windhorst, R. A. 1988, A&A, 195, 21
Kim, K. T., Kronberg, P., Dewdney, P., & Landecker, T. 1990, ApJ, 355, 29
Mewe, R., Gronenschild, E. H. B. M., & van den Oord, G. 1985, A&AS, 62, 197
Miley, G. K. 1980, ARA&A, 18, 165
Miley, G. K., & Harris, D. 1977, A&A, 61, L23
Miley, G. K., Wellington, K. J., & van der Laan, H. 1975, A&A, 38, 381
Mushotzky, R., Serlemitsos, P., Smith, B., Boldt, E., & Holt, S. 1978, ApJ, 225, 21
O'Dea, C., & Owen, F. N. 1985a, AJ, 90, 927
———. 1985b, AJ, 90, 954
———. 1986, ApJ, 301, 841
Perley, R. A., & Taylor, G. B. 1991, AJ, 101, 1623
Roettiger, K., Burns, J., & Loken, C. 1993, ApJ, 407, L53
Roland, J. 1981, A&A, 93, 407
Schwab, F. R. 1984, AJ, 89, 1076
Tribble, P. C. 1991, MNRAS, 250, 726
———. 1993, MNRAS, 263, 31
Valentijn, E. A. 1979, A&A, 78, 367
Vestrand, W. 1982, AJ, 87, 1266
Watt, M. P., Ponman, T. J., Bertram, D., Eyles, C., Skinner, G., & Willmore, A. P. 1992, MNRAS, 258, 738